

Two-dimensional van der Waals electrical contact to monolayer MoSi₂N₄

Liemao Cao,^{1,2} Guanghui Zhou,³ Qianqian Wang,² L. K. Ang,^{2, a)} and Yee Sin Ang^{2, a)}

¹⁾ College of Physics and Electronic Engineering, Hengyang Normal University, Hengyang 421002, China

²⁾ Science, Mathematics and Technology (SMT), Singapore University of Technology and Design (SUTD), 8 Somapah Road, Singapore 487372, Singapore

³⁾ Department of Physics, Hunan Normal University, Changsha 410081, China

Two-dimensional (2D) MoSi₂N₄ monolayer is an emerging class of air-stable 2D semiconductor possessing exceptional electrical and mechanical properties. Despite intensive recent research efforts devoted to uncover the material properties of MoSi₂N₄, the physics of electrical contacts to MoSi₂N₄ remains largely unexplored thus far. In this work, we study the van der Waals heterostructures composed of MoSi₂N₄ contacted by graphene and NbS₂ monolayers using first-principle density functional theory calculations. We show that the MoSi₂N₄/NbS₂ contact exhibits an ultralow Schottky barrier height (SBH), which is beneficial for nanoelectronics applications. For MoSi₂N₄/graphene contact, the SBH can be modulated via interlayer distance or via external electric fields, thus opening up an opportunity for reconfigurable and tunable nanoelectronic devices. Our findings provide insights on the physics of 2D electrical contact to MoSi₂N₄, and shall offer a critical first step towards the design of high-performance electrical contacts to MoSi₂N₄-based 2D nanodevices.

The discovery of monolayer graphene¹ has initiated tremendous experimental and theoretical efforts for the search of new two-dimensional (2D) materials with exotic physical properties and functionalities. One important example is the family of 2D transition metal dichalcogenides (TMDCs), such as MoS₂ and WS₂, whose potential in nanoelectronic², optoelectronic³, photonic⁴, valleytronic⁵ and energy device⁶ applications has revolutionized nanomaterial science and technology in recent years. The potential of 2D TMDCs in industrial-grade 2D nanodevices is further boosted by the enormous design flexibility offered by vertical van der Waals heterostructures (VDWHs) in which physical properties can be custom-made by vertically stacking different 2D atomic layers^{7–11}.

Beyond 2D TMDC, ultrathin transition metal nitride (TMN) have been actively explored in recent years¹². As TMN is a nonlayered material, the experimental synthesis of air-stable and large-area 2D TMN monolayer remains a formidable challenge¹³. In 2020, MoSi₂N₄, a TMN-based monolayer with no known 3D parent structure, has been successfully synthesized using chemical vapor deposition (CVD) method²³, which represents a milestone in the search of 2D TMN-based nanomaterial. MoSi₂N₄, composed of a MoN₂ monolayer sandwiched by two Si-N bilayers, is an indirect bandgap semiconductor with excellent ambient air stability. The intrinsic electron and hole mobilities are predicted to be 270 cm²V⁻¹s⁻¹ and 1200 cm²V⁻¹s⁻¹, respectively, which are substantially higher than that of MoS₂. Density functional theory (DFT) simulation has further revealed an expansive family of MA₂Z₄ monolayers (M = early transition metal, e.g. Mo, W, and Nb; A = Si or Ge, Z = N, P or As), covering semiconducting, metallic and magnetic

phases. The discovery of MoSi₂N₄ and MA₂Z₄ monolayer family thus opens up an uncharted territory for the exploration of 2D-material-based device technology.

Although recent experiment have shed important lights on the structural, electrical, mechanical and optical properties of MoSi₂N₄²³, the physics of electrically contacting MoSi₂N₄ with metals^{26–32} remains largely unknown thus far. In 2D TMDC, their van der Waals (VDW) stacking with 2D metals has led to myriads of unusual characteristics, such as weak Fermi level pinning³⁴, tunable band gap^{35–37}, miniband formation³⁸, and opto-valleytronic spin injection³⁹. In relevance to MoSi₂N₄, the rich physical phenomena already observed in 2D-TMDC/2D-metal contacts immediately lead to the following open questions: Can MoSi₂N₄ be integrated with 2D metals, such as graphene and NbS₂, to form structurally stable VDWHs? What is the electronic properties of such heterostructures? What types of contact, *ohmic* or *Schottky*, are formed in such electrical contacts? Can the contact properties and types be engineered via external tuning knobs such as electric field and interlayer distances?

In this work, we address the above questions by performing a first-principle DFT simulation on the electronic properties of MoSi₂N₄ when it is vertically contacted by 2D metallic electrodes – graphene and NbS₂ monolayers. We find that MoSi₂N₄/NbS₂ Schottky contacts exhibits an ultralow Schottky barrier height (SBH) of 0.042 eV, which is beneficial for room-temperature device operation. For MoSi₂N₄/graphene, the SBH can be controlled by interlayer distance or by external electric field, thus allowing the contact to be reconfigured between *p*-type and *n*-type Schottky contact. As the extended family of MA₂Z₄ contains myriads of 2D monolayers with exotic physical properties yet to be unearthed, our findings shall form a harbinger for designing efficient electrical contact and VDWHs based on MA₂Z₄ monolayer family.

The structural optimization and electronic properties of an isolated monolayer MoSi₂N₄ and its VDWH when

^{a)} Authors to whom correspondence should be addressed: ricky_ang@sutd.edu.sg; and yeemin_ang@sutd.edu.sg

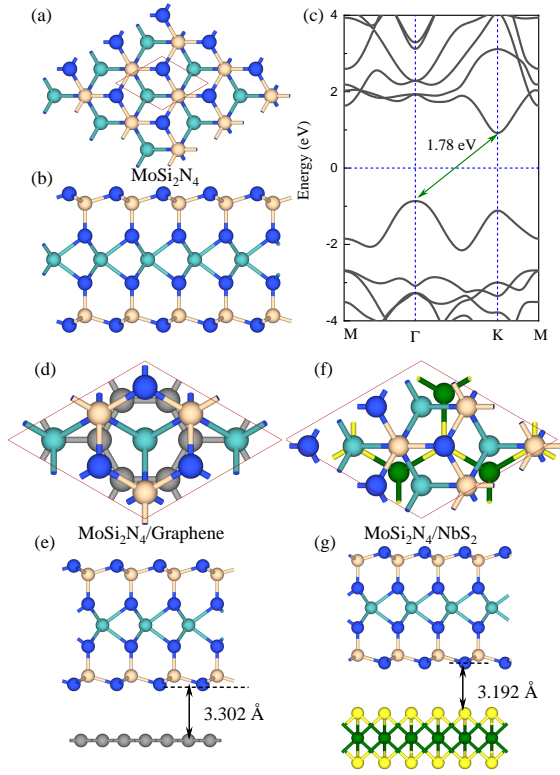


Fig. 1. (Color online) (a) and (b) Top and side view of monolayer MoSi_2N_4 . (c) Band structure of MoSi_2N_4 . (d)-(g) Top and side view of optimized heterostructures of $\text{MoSi}_2\text{N}_4/\text{Graphene}$ and $\text{MoSi}_2\text{N}_4/\text{NbS}_2$.

interfaced with graphene and NbS_2 are performed using the Vienna simulation package (VASP)^{33,40}. The projector-augmented wave (PAW)⁴¹ potentials are used to treat the electron-ion interaction. The generalized gradient approximation (GGA) within Perdew-Burk-Ernzerhof (PBE) pseudopotentials are used to describe the exchange correlation functionals. A cutoff energy of 500 eV is set. DFT-D3 method is used to correct the effect of weak VDW interaction⁴². A vacuum layer (> 20 Å) between the neighboring layers is employed along the z-direction of the heterostructures to eliminate the layer interactions caused by the neighboring slabs. The break criterion for the electronic self-consistency is set to 10^{-6} eV. Monkhorst-Pack k -point grids of $9 \times 9 \times 1$ are chosen. All atoms are fully relaxed using the conjugated gradient method until the force is lower than 0.01 V/Å.

The top and side views of an isolated MoSi_2N_4 are shown in Figs. 1(a) and (b), respectively. The optimized lattice constant for MoSi_2N_4 is $a = b = 2.91$ Å, which is a hexagonal structure with a space group of $P6m1$. MoSi_2N_4 is composed of septuple atomic layers with a thickness of 7.01 Å. Monolayer MoSi_2N_4 exhibits an indirect band gap of 1.78 eV [Fig. 1(c)], compared to that of MoS_2 (1.9 eV) and WS_2 (2.0 eV) monolayers⁵⁸. We further note that the calculations based on PBE functional is closer to the experimental values of 1.94 eV,

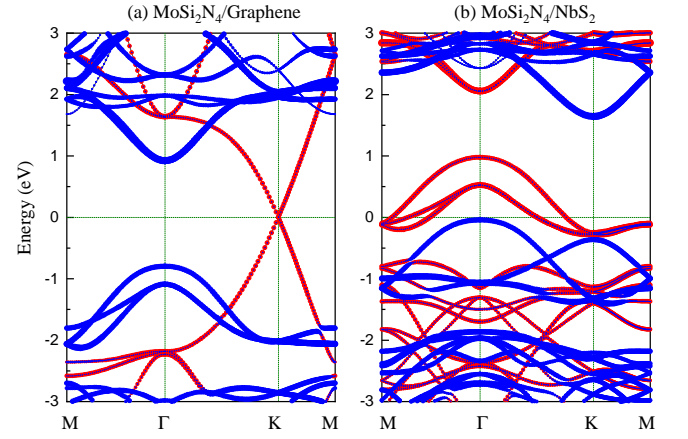


Fig. 2. (Color online) The projected electronic band structures of (a) $\text{MoSi}_2\text{N}_4/\text{Graphene}$ and (b) $\text{MoSi}_2\text{N}_4/\text{NbS}_2$. Here, blue and red symbols denote the contributions from the MoSi_2N_4 and graphene (NbS_2), respectively.

when compared to the HSE06 values of 2.29 eV²³ and 2.35 eV²⁴.

We consider the 2D/2D contacts^{37,43,44} formed by vertically contacting MoSi_2N_4 with graphene and NbS_2 , namely $\text{MoSi}_2\text{N}_4/\text{graphene}$ and $\text{MoSi}_2\text{N}_4/\text{NbS}_2$ VDWHs. We use MoSi_2N_4 $\sqrt{3} \times \sqrt{3}$ and graphene 2×2 supercells to form $\text{MoSi}_2\text{N}_4/\text{graphene}$. For $\text{MoSi}_2\text{N}_4/\text{NbS}_2$, MoSi_2N_4 2×2 and NbS_2 $\sqrt{3} \times \sqrt{3}$ supercells are used [Fig. 1(d)-(g)]. To avoid the properties of MoSi_2N_4 being affected by mechanical stress, we fix the lattice of MoSi_2N_4 and apply strains in graphene and NbS_2 monolayer for $\text{MoSi}_2\text{N}_4/\text{graphene}$ and $\text{MoSi}_2\text{N}_4/\text{NbS}_2$, respectively. The lattice mismatch is 1.6% and 0.07% for $\text{MoSi}_2\text{N}_4/\text{graphene}$ and $\text{MoSi}_2\text{N}_4/\text{NbS}_2$, respectively. The stacking configurations have minimal effect on the physical properties of the heterostructures (see Supplementary Material). After structural relaxation, the interlayer distances are obtained as 3.302 Å and 3.192 Å for $\text{MoSi}_2\text{N}_4/\text{graphene}$ and $\text{MoSi}_2\text{N}_4/\text{NbS}_2$, respectively, which are much larger than the sum of the covalent radii of N and C (S) atoms. The interfaces are found to be dominated by the VDW interactions. We further test the interlayer distances using different VDW functionals (see Supplementary Materials), and the interlayer distances of the fully relaxed structures are found to be similar. We calculated the binding energy E_b as, $E_b = (E_H - E_M - E_{g(n)})/N$ where E_H , E_M , $E_{g(n)}$, and N denotes the total energies of the heterostructures, isolated MoSi_2N_4 , isolated graphene (or NbS_2), and the number of atoms in the heterostructures, respectively. The calculated binding energies are -199.89 eV/atom and -280.29 eV/atom for $\text{MoSi}_2\text{N}_4/\text{graphene}$, and $\text{MoSi}_2\text{N}_4/\text{NbS}_2$, respectively, which are substantially lower than other 2D-material-based heterostructures⁵⁰. Coupled with the excellent mechanical properties of MoSi_2N_4 ²³⁻²⁵, the heterostructures are thus expected to be energetically favorable and stable.

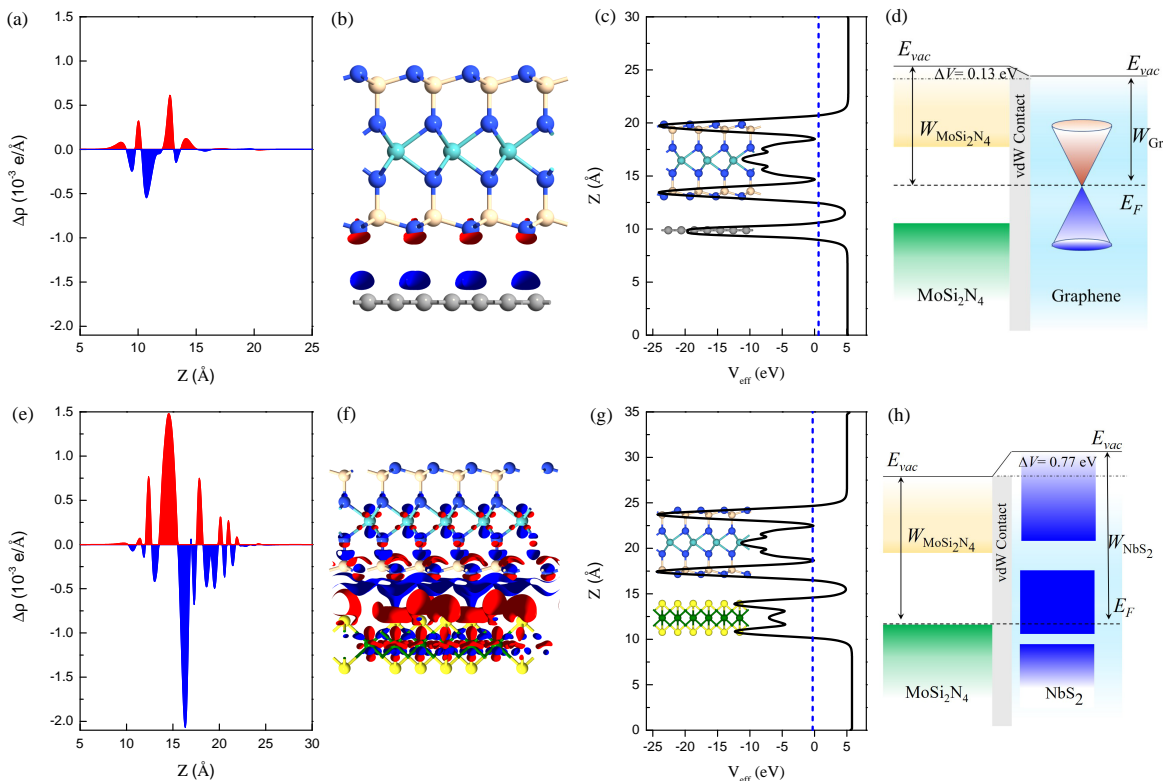


Fig. 3. (Color online) Plane-averaged differential charge density $\Delta\rho$, 3D isosurface of the electron density difference, electrostatic potentials and band diagram of (a-d) MoSi₂N₄/Graphene and (e-h) MoSi₂N₄/NbS₂ heterostructures, respectively.

The projected band structures of MoSi₂N₄/graphene and MoSi₂N₄/NbS₂ (Fig. 2) exhibit no obvious difference when SOC is included (see Supplementary Material). The band structures of MoSi₂N₄, graphene and NbS₂ are well-preserved upon forming the heterostructures. MoSi₂N₄ exhibits a direct band gap in MoSi₂N₄/graphene heterostructure due to band folding, which is a typical feature in 2D VDWs. We determine the SBH via the Schottky-Mott rule⁴⁵, i.e. $\Phi_n = E_{CBM} - E_F$, $\Phi_p = E_F - E_{VBM}$, where Φ_n and Φ_p are the interface potential barrier heights for electrons and holes, respectively; E_{CBM} , E_F and E_{VBM} are the energy of the conduction band minimum (CBM), Fermi energy, and valence band maximum (VBM). For MoSi₂N₄/graphene, the n -type SBH (Φ_n) and the p -type SBH (Φ_p) are 0.922 eV and 0.797 eV, respectively, thus indicating the presence of a p -type Schottky contact. In MoSi₂N₄/NbS₂, the n -type SBH (Φ_n) and the p -type SBH (Φ_p) is 1.642 eV and 0.042 eV, respectively. The ultralow p -type SBH of MoSi₂N₄/NbS₂ contact immediately suggests the potential of NbS₂ as an efficient 2D electrical contact to MoSi₂N₄ with high charge injection efficiency particularly well-suited for room-temperature devices.

We next examine the planar averaged charge density difference and electrostatic potentials of the MoSi₂N₄/graphene and MoSi₂N₄/NbS₂ heterostructures along the z direction (Fig. 3). We define the plane-

averaged differential charge density ($\Delta\rho$) as $\Delta\rho = \rho_H - \rho_M - \rho_{g(n)}$, where ρ_H , ρ_M , and $\rho_{g(n)}$ are the plane-averaged charge density of the heterostructures, isolate plane-averaged charge densities of MoSi₂N₄ and graphene (NbS₂), respectively. The symmetry of the MoSi₂N₄ lattice structure is broken when contacted by graphene and NbS₂, thus leading to charge redistribution. Charge carriers are depleted around the graphene layer while accumulating near the MoSi₂N₄ layer [Figs. 3(a) and (b)]. In contrast, MoSi₂N₄/NbS₂ exhibits excess charges accumulate around the NbS₂ layer while depleting around the MoSi₂N₄ layer. Moreover, the amount of transferred electrons between MoSi₂N₄ and NbS₂ is much greater than that of between MoSi₂N₄ and graphene by direct comparison between Figs. 3(a) and (e). The 3D isosurfaces of the charge density difference is calculated in Figs. 3(b) and (f) for MoSi₂N₄/graphene and MoSi₂N₄/NbS₂, respectively, which clearly illustrate the differences of charge transfer behavior in the two heterostructures. Such charge transfer causes the Fermi level to move towards the valence band of MoSi₂N₄, resulting an ultralow SBH. In Figs. 3(c) and (g), the plane-averaged electrostatic potential difference (V_{eff}) reveals that the direction of built-in electric field is different for the two heterostructures. The corresponding band alignment diagrams of MoSi₂N₄/graphene and MoSi₂N₄/NbS₂ are shown in Figs. 3(d) and (h), respectively.

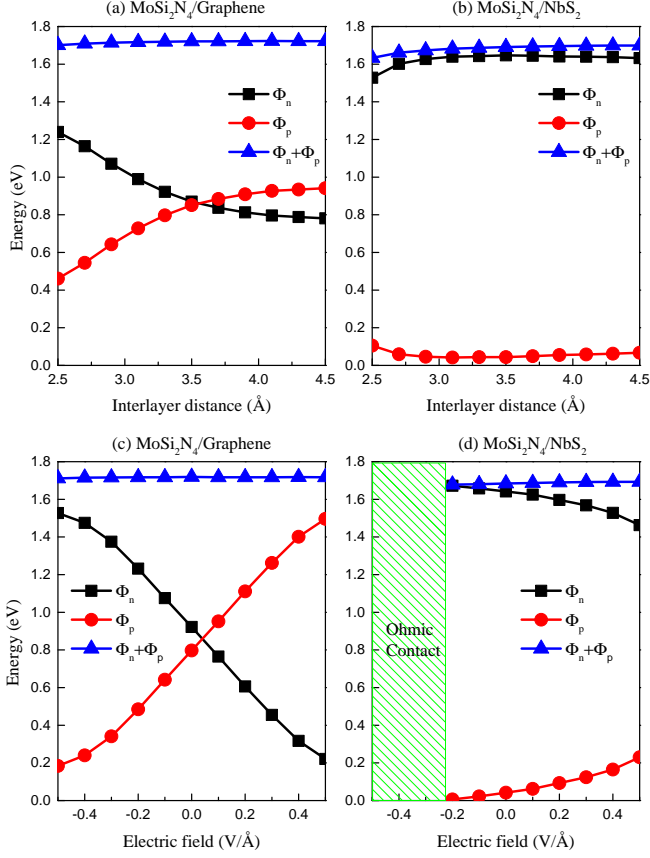


Fig. 4. (Color online) SBH as a function of the interlayer spacing for (a) MoSi₂N₄/graphene and (b) MoSi₂N₄/NbS₂. SBH as a function of external electric field for (c) MoSi₂N₄/graphene and (d) MoSi₂N₄/NbS₂.

Changing the interlayer spacing, which can be achieved experimentally by nanomechanical pressure⁴⁶, diamond anvil cell⁴⁷, vacuum thermal annealing⁴⁸, or by inserting hexagonal BN dielectric layers⁴⁹, provides a viable route to tune the electronic properties of a VDWHS. The SBH of MoSi₂N₄/graphene and MoSi₂N₄/NbS₂ as a function of the vertical strain is illustrated in Fig. 4 [see Supplementary Material for their band structures]. Both electron and hole SBHs of MoSi₂N₄/graphene heterostructure are sensitively influenced by the interlayer distance [Fig. 4(a)]. For instance, an interlayer larger than 3.5 Å signifies the transition from a *p*-type Schottky contact to an *n*-type Schottky contact. In contrary, the SBH of MoSi₂N₄/NbS₂ heterostructure remains robust against interlayer distance variation [Fig. 4(b)].

Electrically tunable electronic properties is a useful characteristics for the design of all-electrical devices^{50–52}. In Figs. 4(c) and (d), we examine the evolution of SBH as a function of an external electric field applied along the *z*-direction of the heterostructures (see Supplementary Material for the band structures). We define the positive direction of the electric field as that pointing from MoSi₂N₄ layer to the 2D metals. For MoSi₂N₄/graphene

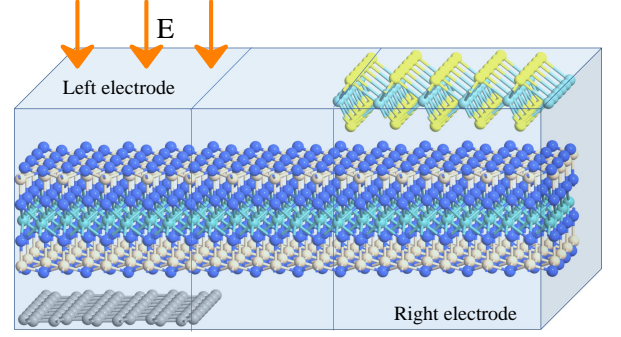


Fig. 5. (Color online) Schematic diagram of a tunable nanodiode device based on a graphene/MoSi₂N₄/NbS₂ heterostructures.

contact, when the external electric field is greater than 0.05 V/Å, the contact is transformed from *p*-type to *n*-type Schottky contact [Fig. 4(c)]. The application of an external electric field thus provide a tuning knob to dynamically control the contact type of MoSi₂N₄/graphene heterostructure. For MoSi₂N₄/NbS₂, the SBH is insensitive to an external electric field [Fig. 4(d)]. When a negative electric field exceeding -0.02 V/Å is applied, the *p*-type SBH is completely eliminated, thus transforming MoSi₂N₄/NbS₂ into an ohmic contact. The SBH tuning originates from the Fermi level shifting in graphene and NbS₂. When the interlayer spacing is changed or when an external electric field is applied, the balance of the system is destroyed. To re-establish equilibrium, the charges redistribute themselves across the interface which changes the Fermi level of contacting graphene and NbS₂^{53,54} and, hence, their work functions. As a result, the SBH is modified.

Finally, we discuss a design of nanodiode composed of MoSi₂N₄/graphene and MoSi₂N₄/NbS₂ electrical contacts. A 2D/2D *homo-lateral p-n* junction can be constructed using a single continuous sheet of MoSi₂N₄, contacted by graphene and NbS₂ on both sides (Fig. 5). The MoSi₂N₄/NbS₂ region becomes *p*-doped, while the MoSi₂N₄/graphene region serves as an electrically tunable contact. By changing the electric field strength and polarity on the MoSi₂N₄/NbS₂, the device can be reconfigured between between *n-p* or *n'-n* nanodiodes. The proposed nanodiodes is composed entirely of a single sheet of MoSi₂N₄ which is in contrast to the lateral⁵⁵ or vertical⁵⁶ heterostructure *p-n* junction composed of two different 2D materials. The lattice mismatch and interfacial carrier scattering effects are expected to be substantially reduced, thus improving the overall charge transport efficiency across the homojunction of the proposed device.

In summary, we investigated the electrical contacts between monolayer MoSi₂N₄ with 2D semimetal (graphene) and 2D metal (NbS₂), using first-principle simulation. Here, the ultralow SBH in MoSi₂N₄/NbS₂ contact can

be a particularly beneficial feature for devices operating at room temperature. For MoSi₂N₄/graphene contact, the SBH can be controlled externally via an electric field or via interlayer distance, thus revealing a potential in reconfigurable device applications. Our findings shall shed important light on the design of MoSi₂N₄-based 2D/2D contacts and heterostructures, thus paving a critical first-step toward the development of VDW heterostructure devices⁵⁹ based on the emerging 2D material family of MA₂Z₄.

SUPPLEMENTARY MATERIAL

See [supplementary material](#) for the complete electronic band structures of MoSi₂N₄ heterostructures under different contact orientation, and the evolution of the electronic band structures under different interlayer distance and external electric fields.

ACKNOWLEDGMENTS

This work is supported by the Singapore MOE Tier 2 Grant (2018-T2-1-007). LC acknowledge the supports of Hunan Provincial Natural Science Foundation of China (Grant No. 2019JJ50016), and science Foundation of Hengyang Normal University of China (No. 18D26). All the calculations were carried out using the computational resources provided by the National Supercomputing Centre (NSCC) Singapore.

Data Availability Statement. The data that support the findings of this study are available from the corresponding author upon reasonable request.

- ¹K. S. Novoselov, A. K. Geim, S. V. Morozov, D. Jiang, Y. Zhang, S. V. Dubonos, I. V. Grigorieva, A. A. Firsov, *Science* **306**, 666 (2004).
- ²G. Fiori, F. Bonaccorso, G. Iannaccone, T. Palacios, D. Neumaier, A. Seabaugh, S. K. Banerjee, L. Colombo, *Nat. Nanotechnol.* **9**, 768 (2014).
- ³Y.-Q. Bie, G. Grosso, M. Heuck, M. M. Furchi, Y. Cao, J. Zheng, D. Bunandar, E. Navarro-Moratalla, L. Zhou, D. K. Efetov et al, *Nat. Nanotechnol.* **12**, 1124 (2017).
- ⁴F. Xia, H. Wang, D. Xiao, M. Dubey, and A. Ramasubramaniam, *Nat. Photon.* **8**, 899 (2014).
- ⁵Y. Ye, J. Xiao, H. Wang, Z. Ye, H. Zhu, M. Zhao, Y. Wang, J. Zhao, X. Yin, and X. Zhang, *Nat. Nanotechnol.* **11**, 598 (2016).
- ⁶E. Pomerantseva and Y. Gogotsi, *Nat. Energy* **2**, 17089 (2017).
- ⁷A. K. Geim and I. V. Grigorieva, *Nature* **499**, 419 (2013).
- ⁸A. C. Ferrari, F. Bonaccorso, V. Fal'ko, K. S. Novoselov, S. Roche, P. Boggild, S. Borini, F. H. L. Koppens, V. Palermo, N. Pugno et al, *Nanoscale* **7**, 4598 (2015).
- ⁹A. Bafekry, M. M. Obeid, C. V. Nguyen, M. Ghergherehchi and M. Bagheri Tagani, *J. Mater. Chem. A* **8**, 13248 (2020).
- ¹⁰A. Bafekry, B. Akgenc, S. Farjami Shayesteh and B. Mortazavi, *Appl. Surf. Sci.* **505**, 144450 (2020).
- ¹¹A. Bafekry and M. Neek-Amal, *Phys. Rev. B* **101**, 085417 (2020).
- ¹²K. Huang, Z. Li, G. Han, and P. Huang, *Chem. Soc. Rev.* **47**, 5109 (2018).
- ¹³X. Xiao, H. Wang, W. Bao, P. Urbankowski, L. Yang, Y. Yang, K. Maleski, L. Cui, S. J. L. Billinge, G. Wang et al, *Adv. Mater.* **31**, 1902393 (2019).
- ¹⁴H. Liu, A. T. Neal, Z. Zhu, Z. Luo, X. Xu, D. Tománek, P. D. Ye, *ACS Nano* **8**, 4033 (2014).
- ¹⁵Q. H. Wang, K. Kalantar-Zadeh, A. Kis, J. N. Coleman, M. S. Strano, *Nat. Nanotechnol.* **7**, 699 (2012).
- ¹⁶B. Feng, J. Zhang, Q. Zhong, W. Li, S. Li, H. Li, P. Cheng, S. Meng, L. Chen, K. Wu, *Nat. Chem.* **8**, 563 (2016).
- ¹⁷M. Naguib, V. N. Mochalin, M. W. Barsoum, Y. Gogotsi, *Adv. Mater.* **26**, 992 (2014).
- ¹⁸K. Khan, A. K. Tareen, M. Aslam, R. Wang, Y. Zhang, A. Mahmood, Z. Ouyang, H. Zhang, Z. Guo, *J. Mater. Chem. C* **8**, 387 (2020).
- ¹⁹M. E. Beck, M. C. Hersam, *ACS Nano* **14**, 6498 (2020).
- ²⁰L. Cao, Y. S. Ang, Q. Wu, L. K. Ang, *Phys. Rev. B* **101**, 035422 (2020).
- ²¹J. Lipton, G.-M. Weng, J. A. Röhr, H. Wang, A. D. Taylor, *Matter* **2**, 1148 (2020).
- ²²X. Li, L. Tao, Z. Chen, H. Fang, X. Li, X. Wang, J.-B. Xu, H. Zhu, *Appl. Phys. Rev.* **4**, 021306 (2017).
- ²³Y.-L. H, Z. Liu, L. Wang, T. Zhou, W. Ma, C. Xu, S. Feng, L. Chen, M.-L. Chen, D.-M. Sun, X.-Q. Chen, H.-M. Cheng, W. Ren, *Science* **369**, 670 (2020).
- ²⁴A. Bafekry, M. Faraji, D. M. Hoat, M. M. Fadlallah, M. Shahrokhi, F. Shojaei, D. Gogova, M. Ghergherehchi, [arxiv:2009.04267v1](#) (2020).
- ²⁵C. Yang, Z. Song, X. Sun, and J. Lu, [arxiv:2010.10764](#) (2020).
- ²⁶A. Venugopal, L. Colombo, E. M. Vogel, *Appl. Phys. Lett.* **96**, 013512 (2010).
- ²⁷Y. S. Ang, H. Y. Yang, and L. K. Ang, *Phys. Rev. Lett.* **121**, 056802 (2018).
- ²⁸D. S. Schulman, A. J. Arnold, S. Das, *Chem. Soc. Rev.* **47**, 3037 (2018).
- ²⁹A. Allain, J. Kang, K. Vanerjee, A. Kis, *Nat. Mater.* **14**, 1195 (2015).
- ³⁰S. Banerjee, L. Cao, Y. S. Ang, L. K. Ang, P. Zhang, *Phys. Rev. Appl.* **13**, 064021 (2020).
- ³¹W. Xiong, C. Xia, X. Zhao, T. Wang, Y. Jia, *Carbon* **109**, 737 (2016).
- ³²Q. Y. Wu, Y. S. Ang, L. M. Cao, and L. K. Ang, *Appl. Phys. Lett.* **115**, 083105 (2019).
- ³³G. Kresse and J. Furthmüller, *Phys. Rev. B* **54**, 11169 (1996).
- ³⁴Y. Liu, P. Stradins, and S.-H. Wei, *Sci. Adv.* **2**, e1600069 (2016).
- ³⁵A. Ebnonnasir, B. Narayanan, S. Kodambaka, and C. V. Ciobanu, *Appl. Phys. Lett.* **105**, 031603 (2014).
- ³⁶F. Zhang, W. Li, Y. Ma, Y. Tang and X. Dai, *RSC Adv.* **7**, 29350 (2017).
- ³⁷L. Cao, Y. S. Ang, Q. Wu, L. K. Ang, *Appl. Phys. Lett.* **115**, 241601 (2019).
- ³⁸D. Pierucci, H. Henck, J. Avila, A. Balan, C. H. Naylor, G. Patriarche, Y. J. Dappe, M. G. Silly, F. Sirotti, A. T. Charlie Johnson et al, *Nano Lett.* **16**, 4054 (2016).
- ³⁹Y. K. Luo, J. Xu, T. Zhu, G. Wu, E. J. McCormick, W. Zhan, M. R. Neupane, and R. K. Kawakami, *Nano Lett.* **17**, 3877 (2017).
- ⁴⁰G. Kresse and J. Furthmüller, *Comput. Mater. Sci.* **6**, 15 (1996).
- ⁴¹G. Kresse and D. Joubert, *Phys. Rev. B* **59**, 1758 (1999).
- ⁴²S. Grimme, J. Antony, S. Ehrlich and H. Krieg, *J. Chem. Phys.* **132**, 154104 (2010).
- ⁴³H. G. Shin, H. S. Yoon, J. S. Kim, M. Kim, J. Y. Lim, S. Yu, J. H. Park, Y. Yi, T. Kim, S. C. Jun, S. Im, *Nano Lett.* **18**, 1937 (2018).
- ⁴⁴X. Ding, S. Zhang, M. Zhao, Y. Xiang, K. H. L. Zhang, X. Zu, S. Li, L. Qiao, *Phys. Rev. Appl.* **12**, 064061 (2019).
- ⁴⁵J. Bardeen, *Phys. Rev.* **71**, 717 (1947).
- ⁴⁶M. Dienwiebel, G. S. Verhoeven, N. Pradeep, J. W. M. Frenken, J. A. Heimberg, and H. W. Zandbergen, *Phys. Rev. Lett.* **92**, 126101 (2004).
- ⁴⁷S. Clark, K.-J. Jeon, J.-Y. Chen, and C.-S. Yoo, *Solid State Commun.*, **154**, 15 (2013).
- ⁴⁸S. Tongay, W. Fan, J. Kang, J. Park, U. Koldemir, J. Suh, D. S. Narang, K. Liu, J. Ji, J. Li, R. Sinclair, and J. Wu, *Nano Lett.* **14**, 3185 (2014).

- ⁴⁹H. Fang, C. Battaglia, C. Carraro, S. Nemsak, B. Ozdol, J. S. Kang, H. A. Bechtel, S. B. Desai, F. Kronast, A. A. Unal, G. Conti, C. Conlon, G. K. Palsson, M. C. Martin, A. M. Minor, C. S. Fadley, E. Yablonovitch, R. Maboudian, and A. Javey, *PNAS* **111**, 6198 (2014).
- ⁵⁰J. E. Padilha, A. Fazio, A. J. R. da Silva, *Phys. Rev. Lett.* **114**, 066803 (2015).
- ⁵¹W. Hu, T. Wang, R. Zhang, J. Yang, *J. Mater. Chem. C* **4**, 1776 (2016).
- ⁵²L. Britnell, R. V. Gorbachev, R. Jalil, B. D. Belle, F. Schedin, A. Mishchenko, T. Georgiou, M. I. Katsnelson, L. Eaves, S. V. Morozov, N. M. R. Peres, J. Leist, A. K. Geim, K. S. Novoselov, L. A. Ponomarenko, *Science* **335**, 947 (2012).
- ⁵³A. Bafekry, C. Stampfl and M. Ghergherehchi, *Nanotechnol.* **31**, 295202 (2020).
- ⁵⁴A. Bafekry, B. Akgenc, M. Ghergherehchi and F. M. Peeters, *J. Phys.: Condens. Matter* **32**, 355504 (2020).
- ⁵⁵M.-Y. Li, Y. Shi, C.-C. Cheng, L.-S. Lu, Y.-C. Lin, H.-L. Tang, M.-L. Tsai, C.-W. Chu, K.-H. Wei, J.-H. He et al, *Science* **349**, 524 (2015).
- ⁵⁶J. E. Padilha, R. H. Miwa, A. J. R. da Silva, A. Fazio, *Phys. Rev. B* **95**, 195143 (2017).
- ⁵⁷C.-H. Lee, G.-H. Lee, A. M. van der Zande, W. Chen, Y. Li, M. Han, X. Cui, G. Arefe, C. Nuckolls, T. F. Heinz et al, *Nat. Nanotechnol.* **9**, 676 (2014).
- ⁵⁸J. Gusakova, X. Wang, L. L. Shiau, A. Krivosheeva, V. Shaposhnikov, V. Borisenko, V. Gusakov, B. K. Tay, *Phys. Status Solidi A*, 1700218 (2017).
- ⁵⁹S.-J. Liang, B. Cheng, X. Cui, and F. Miao, *Adv. Mater.* **32**, 1903800 (2020).